# **Nuclear induction lineshape modeling** via hybrid SDE and MD approach

Cite as: J. Chem. Phys. 159, 124201 (2023); doi: 10.1063/5.0163782 Submitted: 19 June 2023 · Accepted: 10 September 2023 ·









Published Online: 26 September 2023

Mohamad Niknam (D) and Louis-S. Bouchard (1)



# **AFFILIATIONS**

Department of Chemistry and Biochemistry, University of California Los Angeles, 607 Charles E. Young Drive East, Los Angeles, California 90095-1059, USA and Center for Quantum Science and Engineering, UCLA, Los Angeles, California 90095-1059, USA

a) Author to whom correspondence should be addressed: lsbouchard@ucla.edu

#### **ABSTRACT**

The temperature dependence of the nuclear free induction decay in the presence of a magnetic-field gradient was found to exhibit motional narrowing in gases upon heating, a behavior that is opposite to that observed in liquids. This has led to the revision of the theoretical framework to include a more detailed description of particle trajectories since decoherence mechanisms depend on histories. In the case of free diffusion and single components, the new model yields the correct temperature trends. The inclusion of boundaries in the current formalism is not straightforward. We present a hybrid SDE-MD (stochastic differential equation - molecular dynamics) approach whereby MD is used to compute an effective viscosity and the latter is fed to the SDE to predict the line shape. The theory is in agreement with the experiments. This two-scale approach, which bridges the gap between short (molecular collisions) and long (nuclear induction) timescales, paves the way for the modeling of complex environments with boundaries, mixtures of chemical species, and intermolecular potentials.

Published under an exclusive license by AIP Publishing. https://doi.org/10.1063/5.0163782

## I. INTRODUCTION

During the mid-20th century, when the first nuclear magnetic resonance (NMR) experiments were performed in liquids, magneticfield inhomogeneity was the limiting factor that determined the properties of nuclear induction. Rapid signal decay is problematic on so many levels, especially because it limits spectral resolution. This led to the development of the Hahn echo, where the effects of external magnetic field inhomogeneity are removed by a  $\pi$ rotation about the x axis in a time-reversal experiment. Spin echoes enabled more accurate studies of intrinsic spin-spin relaxation mechanisms and molecular structures. Years later, the deliberate creation and modulation of magnetization by magnetic-field gradients formed the basis of modern techniques in magnetic resonance imaging (MRI).

Given the ubiquitous nature and uses of magnetic-field gradients in modern magnetic resonance experiments, it is imperative that the nuclear response function and its dependence on the sample under study in the presence of applied gradients be properly understood. A correct understanding of the true limits and capabilities of the experiment will enable accurate interpretation of the experimental results as well as inform future developments and applications. In

organic and biological chemistry, for example, NMR spectroscopy is routinely used as a tool to analyze solution content and composition for chemical species' identities and relative content. Limiting factors that compromise linewidth must be minimized or removed so that spectra can be obtained of sufficiently high resolution to elucidate molecular structures. The diffusion of molecules can cause undesirable effects such as altering line shape or be used advantageously, for example, by helping probe transport phenomena. While diffusion can sometimes lead to sharper lines (e.g., increased spectral resolution due to diffusional averaging of the intermolecular magnetic dipole interaction), the presence of residual gradients does create a complex relationship between nuclear induction and sample properties and geometry that obscures the interpretation of results that rely on line shape analysis. Diffusion-weighted readouts have enabled imaging of gases in lungs,4 operando monitoring of chemical reactions,5-<sup>-7</sup> as well as biophysical or mechanical properties of gels and biological tissues.<sup>8,9</sup> In materials science and engineering, diffusion processes are essential to fabrication and synthesis.

In light of these various effects, the observation that in gases lines become narrow with temperature was rather surprising given that the conventional theory predicted a broadening instead. 1,12-14 In liquids, a broadening is observed experimentally, and this is in agreement with theory. This led to a revision of the line shape theory in gases accounting for the time history of rapid molecular motions below the timescale of the NMR experiment. 15 It is critical to account for the history of molecular motions when the process involves motional averaging due to collisions. Conventional theory ignores the histories of molecular diffusion and instead assumes a Gaussian probability distribution for the accumulated phase of the spins. The Gaussian assumption on phase accumulation, which neglects the details of molecular trajectories, only appears justified in liquids, where many collisions occur on the NMR timescale. However, in gases, the average separation between molecules is much larger, and this assumption is more difficult to justify. A drawback of the new theory is its increased complexity. While it provides good agreement between theory and experiments in the case of free diffusion, it is unclear how one should model the effects of realistic boundaries. Stochastic differential equations (SDE) can be used to model molecular trajectories, but this still requires validation against experiments.

In this study, we bridge the gap by using molecular dynamics (MD) simulations and coupling them to an SDE in order to describe nuclear induction. By modeling the viscosity of fluids using MD, the line shape is then derived from the viscosity via its connection to the SDE. Our simulations of particle collisions and trajectories using Lennard-Jones (LJ) interaction reveal opposite trends in liquid and gas particle viscosity coefficients as a function of temperature. This, in turn, can be used to describe the line shape trends in gases and liquids. This work establishes the feasibility of the hybrid SDE-MD approach and paves the way for modeling complex interactions with boundaries and other components. The advantages of modeling viscosity by MD include the possibility of including realistic boundaries, multiple components, or varying the details of intermolecular interactions. Indeed, models of effective viscosity have already been developed for such situations. <sup>16–19</sup>

# A. Review of conventional theory

Assume that an ensemble of spins is placed in an external magnetic field and that a coherent superposition between the states  $|\uparrow\rangle$  and  $|\downarrow\rangle$  is created. In an inhomogeneous field, the phase accumulation for each spin is proportional to the local field experienced by the spin over time. Phase accrued by nuclear spins can be refocused by the application of a  $\pi$  pulse, which inverts the direction of spin rotations, or by simulating a "time-reversal," forming a Hahn echo. 1,20–23 If the spins are fixed (frozen) in space, evolution is described with a unitary propagator, and the entropy remains constant. With diffusion (e.g., liquids and gases), not all initial phases within a spin ensemble can be recovered, and the Hahn echo signal will be smaller. Assuming that the molecules undergo a random walk, it has been postulated that they sample random phase increments from a Gaussian distribution. In the presence of a magnetic-field gradient  ${\bf g}$ , the phase accrued by a spin from time 0 to t is

$$\Delta\phi(t) = \int_0^t \omega(t')dt' = \gamma_n \int_0^t \mathbf{g} \cdot \mathbf{r}(t')dt', \tag{1}$$

where  $\omega(t)$  is the time-dependent frequency of a moving spin,  $\gamma_n$  is the nuclear gyromagnetic ratio, and  $\mathbf{r}(t)$  is the time-dependent position of the diffusing particle. The nuclear induction signal is

weighted by the ensemble average of these phase factors, written with the probability distribution  $P(\Delta \phi)$ ,

$$\langle \exp(i\Delta\phi(t))\rangle = \int_{-\infty}^{\infty} P(\Delta\phi) \exp(i\Delta\phi) d(\Delta\phi).$$
 (2)

To alleviate the notation, we will drop t from the notation and write  $\Delta \phi(t) = \Delta \phi$ . Assuming a Gaussian distribution for  $P(\Delta \phi)$  with variance  $\langle (\Delta \phi)^2 \rangle$  proportional to t, we get

$$S(t) = \langle \exp(i\Delta\phi) \rangle = \exp(-\langle (\Delta\phi)^2 \rangle / 2).$$

Therefore, for the free diffusion under a steady magnetic field of a linear gradient  $\mathbf{g}$  and duration t, the attenuation of the NMR signal S(t) was found to be

$$S(t) = \exp[(-1/3)\gamma_n^2 g^2 D t^3],$$
 (3)

where D is the self-diffusion coefficient, and the  $t^3$  decay arises from self-diffusion in the presence of a field gradient. <sup>23,24</sup> This equation shows that for unrestricted diffusion, as D gets larger, a wider range of  $\Delta\phi$  is sampled resulting in faster damping of the signal. In the Hahn echo experiment,  $90^\circ - \tau - 180^\circ - \tau$ , at  $t = 2\tau$ , the decay function is similar,

$$S(2\tau) = \exp\left(-\frac{2}{3}\gamma_n^2 g^2 D \tau^3\right). \tag{4}$$

The  $t^3$  dependence has been validated experimentally for liquids. This form of signal can be used to describe a Carr–Purcell–Meiboom–Gill (CPMG) experiment with n refocusing  $\pi$  pulses and an interpulse delay of  $2\tau$ . The signal at  $t=2n\tau$  decays according to

$$S(2n\tau) = \exp\left(-\frac{2}{3}\gamma_n^2 g^2 D\tau^2(n\tau)\right). \tag{5}$$

As a result, the signal attenuation at time  $t = 2n\tau$  can be reduced by decreasing the time delay between the pulses  $\tau$  while increasing the number of pulses n. Equations (4) and (5) have been extensively validated in experiments for the case of liquids. The assumption of Gaussian-distributed phase increments is reasonable for liquids because of the short mean-free paths and the large number of collisions during time intervals of duration  $\tau$ .

## B. Problems with conventional theory

In the case of gas molecules, which are characterized by longer mean free paths, the assumption of randomly distributed phase increments becomes more difficult to justify. <sup>10,26</sup> Two simple arguments can be used to illustrate the need for a more sophisticated model. The first one is the observation that in the series expansion of the phase factor

$$\left\langle \exp\left(i\int_0^t \omega(t')dt'\right)\right\rangle = 1 + i\int_0^t \langle \omega(t')\rangle dt' + (i)^2 \int_0^t dt' \int_0^t \langle \omega(t')\omega(t'')\rangle dt'' + \cdots,$$

computation of *n*-point time autocorrelation functions such as  $\langle \omega(t_1) \dots \omega(t_n) \rangle$  requires *n*-point joint probability distributions

such as  $p_{t_1,t_2,...,t_n}(x_1,x_2,...,x_n)$ . Failure to do this is equivalent to neglecting time correlations in the stochastic process  $\{\omega(t)\}$ , which are imposed by the physics of molecular motions and collisions. For the second argument, we model the velocity process as memoryless Brownian motion (Ornstein–Uhlenbeck),

$$dv = -\gamma v dt + \frac{\Gamma_f}{M} dW(t),$$

where  $\gamma^{-1}$  is a damping time constant and dW(t) is the increment of the Wiener process W(t) at time t (dW(t) := W(t) - W(t - dt)). The strength of fluctuations is  $\Gamma_f = \sqrt{2\gamma Mk_BT}$  (fluctuation-dissipation theorem), where M is the mass of the diffusing particle and  $k_B$  is the Boltzmann constant. After integration

$$v(t) = \langle v(t) \rangle + \sqrt{\frac{2\gamma k_B T}{M}} e^{-\gamma t} \int_0^t e^{\gamma t'} dW(t'),$$

where  $\langle v(t) \rangle = \langle v_0 \rangle e^{-\gamma t}$ . The position process is the time integral of the velocity process, dx(t) = v(t)dt, whose solution is [setting x(0) = 0]

$$x(t) = \frac{v_0}{\gamma} (1 - e^{-\gamma t}) + \sqrt{\frac{2\gamma k_B T}{M}} \int_0^t dt' e^{-\gamma t'} \int_0^{t'} dW(t'') e^{\gamma t''}.$$

Because x(t) is given by a sum of Gaussian-distributed increments, dW(t), x(t) is also Gaussian. Its mean is  $\frac{v_0}{\gamma}(1-e^{-\gamma t})$ . Defining a thermal velocity  $v_T = \sqrt{k_B T/M}$ , its second moment is

$$\sigma_x^2(t) := \frac{2v_T^2}{\gamma}t - \frac{v_T^2}{\gamma^2}(3 - 4e^{-\gamma t} + e^{-2\gamma t}).$$

Therefore, the distribution of x(t) is [again, assuming x(0) = 0]

$$p(x,t) = \frac{1}{\sqrt{2\pi\sigma_x^2(t)}} \exp\left[-\frac{(x - v_T(1 - e^{-\gamma t})/\gamma)^2}{2\sigma_x^2(t)}\right].$$

At short t, this is not the usual Gaussian with variance t characteristic of long-time particle diffusion (i.e., the Einstein–Fick limit). Only at long times ( $t \gg \gamma^{-1}$ ) does the distribution become Gaussian with variance t,

$$p(x,t) \to \frac{1}{\sqrt{4\pi Dt}} \exp \left[ -\frac{(x - v_T/\gamma)^2}{4Dt} \right],$$

with diffusion coefficient  $D = k_B T/M \gamma$ . To compute the accrued phase, which is a time integral of x(t) [cf. Eq. (1)], it appears prudent to model the behavior at short times  $(t \lesssim \gamma^{-1})$ . The timescale  $\gamma^{-1}$  of the friction coefficient is associated with molecular collisions.

It has been shown<sup>10</sup> that Eqs. (4) or (5) do not describe the nuclear induction decay in gases. Instead, it was observed that in the CPMG experiment,

$$\langle \exp(i\Delta\phi)\rangle = \exp(-\gamma^2 g^2 \kappa (2n\tau)).$$
 (6)

Here, the decay constant  $\kappa$  is a decreasing function of temperature T, damping rate  $\gamma$ , and particle mass M, Eq. (18). Notice the different powers of  $\tau$  inside the argument of the exponential function ( $\tau^3$  vs  $\tau$ ). This difference was first noticed by observing the

linewidth dependence on temperature  $^7$  and was subsequently investigated more in-depth in Refs. 10 and 26. The conclusion from these studies is that a more detailed description of diffusion effects is needed. Obviously, exact solutions to the N-body problem are not possible; hence, we seek suitable models.

## C. Generalized Langevin equation (GLE)

The GLE is a well-established model of particle diffusion that accounts for memory effects as the molecules undergo diffusion via collisions. In the gas and liquid phases, nuclear spin degrees of freedom are fairly well isolated from spatial degrees of freedom, at least to the first order. Consequently, individual molecular collisions do not completely depolarize the spins. Instead, decoherence and depolarization processes, which are second-order processes, take place over much longer periods of time. Decoherence is described by a characteristic decay time  $T_2$ . The motional part of the NMR signal can thus be written as the expectation value of the spin phase factors [cf. Eq. (1), with  $\omega(t) = \gamma_n g \cdot x(t)$  in 1-D], which depends on their position x(t). In Ref. 10, it is assumed that x(t) is a Gaussian random process that is stationary in the wide sense. The expectation value

$$S(t) = \left\langle \exp\left(i \int_0^t \omega(t') dt'\right)\right\rangle,\tag{7}$$

takes the form

$$\exp\left[i\gamma_n g \int_0^t \langle x(t')\rangle dt' - \gamma_n^2 g^2 \int_0^t \langle x(t')x(0)\rangle (t-t') dt'\right]. \tag{8}$$

The second term determines the line shape of the signal decay. For liquids, displacements are small  $x(t) \approx x(0)$ , and this leads to the Einstein–Fick limit  $\langle x(t)x(0)\rangle \approx \langle x(t)x(t)\rangle = 2Dt$ , where D is a diffusion coefficient, and the classic Hahn result (3) is recovered.

We note that there is no easy way to compute the integral over the function  $\langle x(t')x(0)\rangle$  from first principles in the general case of arbitrary physical conditions. Even MD simulations fail because  $\langle x(t')x(0)\rangle$  decays on short time scales (tens to hundreds of picoseconds) before reaching a nonzero steady state value, after which the time integral is weighted by the monotonically increasing weight (t-t')dt' over much longer time scales (microseconds to seconds). The initial decay and any numerical errors associated with it are then amplified by orders of magnitude. Instead, a model is needed that bridges the two widely different timescales by analytically solving the integral and reducing it to a function of transport coefficients that are easier to compute. Such a transformation was first presented in Ref. 7. The main steps of its derivation, although well known to the fluid dynamics community, are recapped below for convenience.

In the "weak collision" regime (see Ref. 10), a GLE with a memory kernel describes particle dynamics,

$$M\dot{v} + \int_0^t \Gamma(t - t')v(t')dt' = \eta_f(t), \tag{9}$$

where M is the mass of diffusing particle,  $v(t) = \dot{x}(t)$  and  $\dot{v}$  are particle velocity and acceleration.  $\eta_f(t)$  on the right-hand side represents a time-dependent stochastic force. The memory kernel  $\Gamma(t)$  is convoluted with the particle velocity to describe the friction asserted by the viscous dynamics.

Projecting both sides of the GLE equation with the inner product  $\langle v(0), \cdot \rangle$ , we get

$$M\langle v(0)\dot{v}(t)\rangle + \int_0^t \Gamma(t-t')\langle v(0)v(t')\rangle dt' = 0.$$
 (10)

Note that  $\langle v(0)\eta_f(t)\rangle = 0$ , since the stochastic force at t > 0 is independent of the initial velocity by causality. This equation can be recast in terms of the integral of the velocity autocorrelation function,  $v(t) = \int_0^t \langle v(0)v(t')\rangle dt'$ . The equipartition theorem yields  $\langle v(0)v(0)\rangle = k_B T/M$ . The resulting equation for  $v(t)^{27}$  is

$$M\dot{v}(t) + \int_0^t \Gamma(t - t')v(t')dt' = k_B T. \tag{11}$$

Time correlation functions such as the velocity autocorrelation function and related transport coefficients can be found by solving this integro-differential equation. For the memory kernel, one often invokes the Ornstein–Uhlenbeck process to model the delayed response of surrounding fluid,

$$\Gamma(t) = (\gamma^2/m) \exp(-\gamma t/m), \tag{12}$$

where  $\gamma$  is a friction coefficient proportional to the viscosity of the fluid and m represents a mass attributed to solvent particles. The solution using  $\zeta_{\mp} = \frac{\gamma}{2m} (1 \mp \sqrt{1-4 \ m/M})$  is

$$v(t) = \frac{k_B T}{M} \left( \frac{\gamma}{m \zeta_- \zeta_+} + \frac{1}{\zeta_+ - \zeta_-} \left[ \left( 1 - \frac{\gamma}{m \zeta_+} \right) \exp\left( -\zeta_+ t \right) \right. \right.$$
$$\left. - \left( 1 - \frac{\gamma}{m \zeta_-} \right) \exp\left( -\zeta_- t \right) \right] \right). \tag{13}$$

In addition, since  $\langle v(t)v(0)\rangle = -\frac{d^2}{dt^2}\langle x(t)x(0)\rangle$ , the position auto-correlation function is found by integrating the velocity autocorrelation function twice,

$$\langle x(t)x(0)\rangle = \frac{k_B T}{M(\zeta_+ - \zeta_-)} \left[ \zeta_+^{-1} \left( 1 - \frac{\gamma}{m\zeta_+} \right) \exp\left( -\zeta_+ t \right) \right] \times \zeta_-^{-1} \left( 1 - \frac{\gamma}{m\zeta_-} \right) \exp\left( -\zeta_- t \right).$$
(14)

In the case that  $\gamma t/m$  is sufficiently large, the Ornstein–Uhlenbeck kernel rapidly decays. At this point, it is possible to introduce a dependence on viscosity by invoking Stokes' drag law  $\gamma = 6\pi\eta R$ , where R is the radius of the "Brownian particle" and  $\eta$  is the shear viscosity. The validity of Stokes' law is predicated on the assumption that the Brownian particle is much larger than the solvent particles  $(M\gg m)$ . In the case of self-diffusion, all particles are identical. Hence, Stokes' law appears unjustified. However, the proportionality between  $\gamma$  and  $\eta$  is always correct. In fact, Einstein developed the concept of "effective viscosity," which has been used to describe the effective viscosity of lubricants.

We are now in a position to replace the integral in Eq. (8) by a function of the viscosity, a transport coefficient that is easily computed from MD simulations with good accuracy. Viscosity is essentially a coarse-grained quantity describing the relaxation of momentum density to its equilibrium value after a perturbation. It is directly related to the velocity auto-correlation function. Stokes'

law has been extended to the frequency domain to describe dynamical and dissipative effects in rheology.  $^{32-34}$  The relationship between the Fourier representation of frequency dependent viscosity and the frequency-dependent friction coefficient  $\tilde{\gamma}(s)$  is

$$\tilde{\eta}(s) = \frac{\tilde{\gamma}(s)}{6\pi R},\tag{15}$$

where s is the complex frequency in Laplace domain and  $\tilde{p}(\omega) = \int_0^\infty \Gamma(t) \exp{(i\omega t)}.^{32}$  This relationship, which has been termed the "correspondence principle,"<sup>34</sup> provides a direct link between memory function and viscosity. The memory kernel itself encodes the response of particles at all frequencies to collisions and boundary conditions. Therefore, we expect the viscosity to be sensitive to boundary conditions and intermolecular potentials as well. In particular, we expect that changes in the line shape of the NMR signal, cf. Eq. (7), as a function of temperature will be reflected in the memory function as well as the viscosity coefficient.

The case of gases. A model for the viscosity and its temperature dependence is needed.<sup>35</sup> The dynamic viscosity of gases was described by Sutherland as

$$\eta = \frac{\mu_0(T_0 + C)}{T + C} \left(\frac{T}{T_0}\right)^{3/2} \sim \frac{T^{3/2}}{T + C},\tag{16}$$

where *C* is Sutherland's constant and  $\mu_0$  is the viscosity at temperature  $T_0$ . At high temperatures, viscosity grows with the square root of the temperature,  $\eta \sim T^{1/2}$ , while at low temperature,  $\eta \sim T^{3/2}$ . Using Stokes' drag law, we rewrite the nuclear induction signal as<sup>10</sup>

$$S(t) = \exp\left(-\gamma_n^2 g^2 \kappa t\right),\tag{17}$$

with

$$\kappa(T) = \frac{k_{\rm B}T(-m\zeta_{-}^{2}\zeta_{+} - m\zeta_{-}\zeta_{+}^{2} + \zeta_{-}^{2}\gamma + \zeta_{-}\zeta_{+}\gamma + \zeta_{+}^{2}\gamma)}{mM\zeta_{-}^{3}\zeta_{+}^{3}}$$

$$= \frac{k_{\rm B}TM(M + 3m(-1 + \pi R\eta))}{27\pi^{3}R^{3}\eta^{3}}.$$
 (18)

Note that  $\kappa$  determines the linewidth  $\Delta f$ , and it shows two distinct trends with temperature,

$$\Delta f \sim \begin{cases} T^{-7/2} & T < C, \\ T^{-1/2} & T > C. \end{cases}$$
 (19)

Figure 1 represents the decay of the gas phase NMR signal in an echo experiment for a range of temperatures. The sample is a sealed tube of liquid tetramethylsilane (TMS) prepared using the freeze-pump-thaw method. The sample tube is heated above 25 °C to evaporate the TMS. Measurements were performed on a Bruker AV 600 MHz NMR spectrometer equipped with variable temperature and pulsed gradient capabilities. In the presence of a magnetic-field gradient, the line narrows with increasing temperature, a surprising result that was first observed and explained in Refs. 7, 10, and 11. Data points are fitted to exponential decay functions according to Eq. (17), and the resulting linewidths are plotted in the inset of Fig. 1. Their temperature trend is in agreement with Eq. (19).

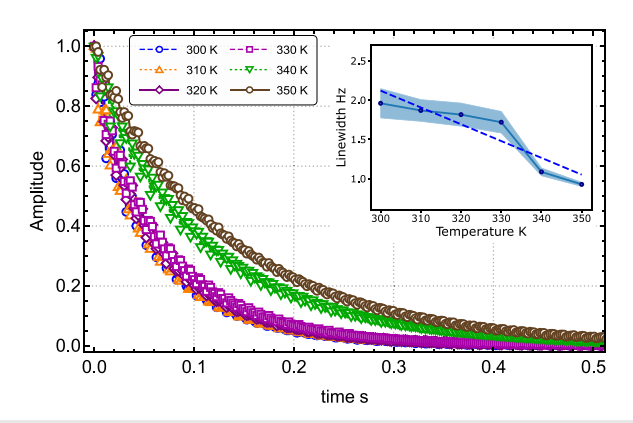


FIG. 1. The decay of the NMR echo signal for TMS in the gas phase for a variable temperature at g = 0.01 G/cm. The decay becomes slower at higher temperatures. The inset indicates the linewidth  $\Delta f \propto \kappa(T)$ , extracted by fitting the time domain data to an exponential decay function Eq. (17). The dashed line shows the best fit using  $\kappa(T) = cT^{-1/2}$ , where c is a constant. Error bars show the standard error obtained from parameter fitting.

The case of liquids. To model the viscosity of liquids, an empirical equation of the form

$$\eta = A \exp(B/T),\tag{20}$$

where A and B are constants that can be substituted into the expression for the nuclear induction decay [cf. Eq. (17)]. Recalling that  $\kappa(T)$  is proportional to  $T\zeta^{-3}$ , we find

$$\kappa(T) \propto T \exp(-3B/T) = T(1 - 3B/T + \frac{9}{2}B^2/T^2 + \cdots).$$

The overall temperature dependence of the linewidth is a line broadening with increasing temperature. 7,10,11 In any case, these equations are only models for  $\eta$ . They do not account for boundaries, yet it is known that boundaries alter the effective viscosity.<sup>28–31</sup> Therefore, the problem has been reduced to the modeling of an effective viscosity.

#### **II. MD RESULTS**

MD simulations of particle trajectories have been used to model gas diffusion in systems of gas mixtures in complex geometries. In particular, for liquids and non-ideal gases whose transport properties are difficult to describe, MD simulations have proven very successful. 16-18 The MD simulations take the free volume model into account in order to describe atom dynamics as a sequence of collisions resembling hard spheres, possibly leading to localized mass movement. The free volume model's parameters can be inferred from microscopic characteristics, and it is capable of explaining variations in transport properties with temperature.19

At each time step, intermolecular forces between the nearest neighbors are enforced to recreate realistic particle trajectories.3 To obtain such trajectories over a large number of particles, we used the open source software "Large-scale Atomic/Molecular Massively Parallel Simulator" (LAMMPS).41 LAMMPS results were then used to compute viscosity coefficients in liquid and gaseous xenon (Xe). We used the Lennard-Jones (LJ) pairing,  $U(r) = 4\epsilon [(\sigma/r)^{12}]$  $-(\sigma/r)^6$ ], where  $\epsilon = 1.77$  kJ/mol is the depth of the potential well and  $\sigma = 4.1$  Å is the distance where the potential is zero. Simulations were performed for 1000 Xe atoms in a box with periodic boundary conditions. The simulations ran for a constant number of particles, volume, and temperature in the canonical ensemble (NVT). The equilibrium time correlation function approach, a.k.a. the Green-Kubo auto-correlation function, was used to derive the viscosity,

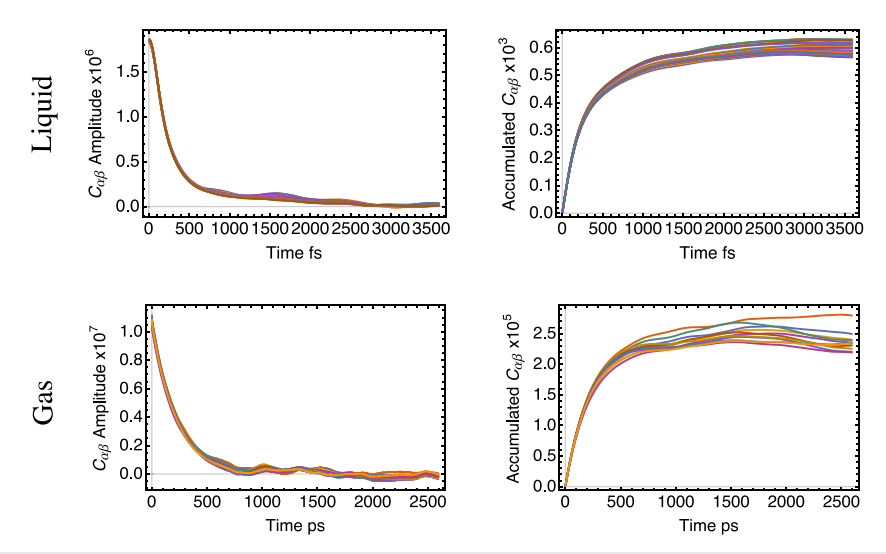
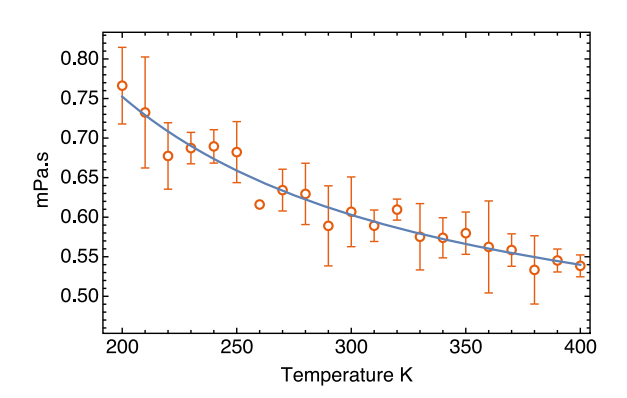


FIG. 2. Green-Kubo correlation functions for liquid and gas simulations are evaluated at each temperature for both densities. Here, the simulation results at 300 are presented (left). These correlations are integrated to the saturation point to evaluate the viscosity coefficient equation (22) (right). Note that the time axis is three orders of magnitude larger for gas simulations.



**FIG. 3.** Viscosity in liquids drops as the temperature increases. Error bars indicate the standard deviation for the set of 60 accumulated correlation functions. The solid line is a fit to Eq. (20) with  $A=0.38\pm0.01$  and  $B=135\pm7$ .

$$\eta = \lim_{t \to \infty} \eta_{GK}(t) \tag{21}$$

with

$$\eta_{GK}(t) = \frac{V}{3k_B T} \int_0^t \sum_{\alpha < \beta} C_{\alpha\beta}(\tau) d\tau, \qquad (22)$$

where  $\alpha, \beta \in \{x, y, z\}$ , V is the volume, and T is the temperature.  $C_{\alpha\beta}(\tau) = \langle p_{\alpha\beta}(\tau) p_{\alpha\beta}(0) \rangle$  is the auto-correlation function of non-diagonal elements of the pressure tensor, e.g.,

$$p_{xy}(t) = \frac{1}{V} \left\{ \sum_{j} m_{j} v_{jx}(t) v_{jy}(t) + \frac{1}{2} \sum_{i \neq j} r_{ijx}(t) f_{ijy}(t) \right\}.$$

Here,  $f_{ijy}$  represents the *y*-component of the force between two particles *i* and *j*. The first term on the right hand side is the kinetic contribution to the pressure tensor, while the second term indicates the potential contribution. Other components  $p_{\alpha\beta}$  of the pressure tensor are defined analogously.

Simulations were performed for 21 different temperature values in the range 200–400 K, using a high density ( $\rho = N/V$ ) of

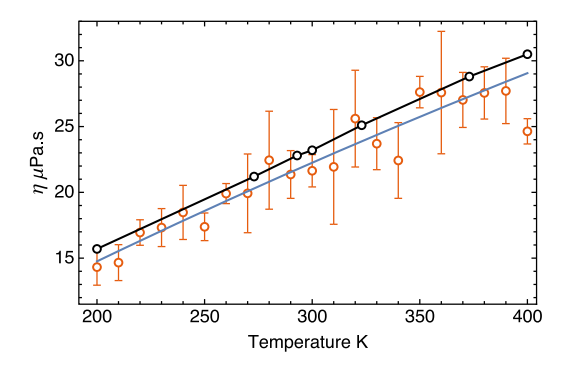


**FIG. 4.** Viscosity in gas molecules grows as the temperature increases. Red circles indicate the results of MD simulations, and black circles are experimental data. Error bars are the standard deviation for the set of 60 accumulated correlation functions. The solid line shows a fit to Eq. (16) with  $C=258\pm69$ .

particles compatible with the liquid phase and a low density for the gas phase. Particle trajectories evolved for  $10^6$  fs to equilibrate. We evaluated  $C_{\alpha\beta}$  correlation functions 60 times in each simulation, recording them well beyond their saturation point (see Fig. 2). They were then used to evaluate the Green–Kubo integral Eq. (21). For this approach to work, it is critical that the correlation functions decay at similar rates so that the resulting integrals converge to an average value.

The shear viscosity coefficient for the liquid state was found to decrease with temperature (see Fig. 3). This behavior is expected and well understood for liquids and is in agreement with the line broadening observed in the liquid state NMR experiments. The verification of simulated viscosity coefficients against experimental values is complicated by the fact that Xe is not in liquid form above 270 K, whereas below that temperature, measurements report viscosity vs temperature but across different densities. A4,45 Nevertheless, a matching data point exists: at 220 K, our simulated viscosity coefficient lies within 5% of the experimentally measured value. Our simulation results are similar to those from Ref. 46, where the authors performed a general study of LJ potential dynamics vs  $\rho$  and T and found that the resulting viscosity coefficients are within 6% of experimental values. The decay of  $\eta(T)$  with T was found to be exponential and was fitted to Eq. (20).

The gas phase simulations were performed by first equilibrating the system over a period of  $10^6$  ps. Compared to the liquid case, the correlation functions were found to decay slower as the frequency of particle collision is smaller (see Fig. 2). The simulated viscosity values were found to be two orders of magnitude smaller as well. Moreover, viscosity coefficients in gases show the opposite trend to those of liquids, i.e., shear viscosity increases with temperature (Fig. 4). A comparison to the available experimental data 47,48 shows that the simulated viscosity coefficients overlap with them. The calculated viscosity coefficients are fitted to Eq. (16). We find that Sutherland's constant ( $C = 258 \pm 69$ ) is in agreement with the literature value for Xe gas (C = 252).

Our MD results confirmed that as the temperature of gases increases, the higher frequency of molecular collisions results in greater resistance and larger viscosities. Viscosity results are

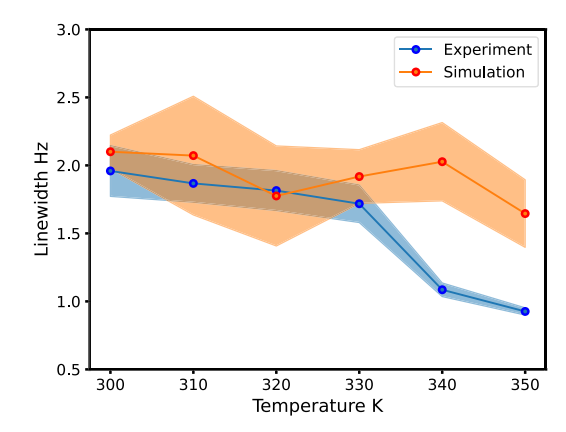


**FIG. 5.** Temperature dependence of nuclear induction linewidth for Xe gas. Experimental data are compared with linewidths calculated for MD-derived viscosity coefficients using Eq. (18).

in agreement with previous studies and experimental results, as expected. On the other hand, what is new here is our ability to predict the correct line shape for the nuclear induction signal from MD results, and this line shape is predicted based on the effective viscosity. Equation (18) suggests that the decay rate of the nuclear induction signal is inversely proportional to the viscosity coefficient  $\eta$ , and as a result, the linewidth narrows at higher temperatures. A depiction of such behavior for the experiment with g = 0.01 G/cm is shown in Fig. 5, where the simulated viscosity coefficients were used to predict the line shape in gases. The resulting linewidths are very close to the experimental values of Fig. 1. A side-by-side comparison of experiments and theory is shown in Fig. 5.

# III. CONCLUSION

We have shown the feasibility of using MD simulations to model transport coefficients in liquids and gases; these transport coefficients are then used together with a GLE model to obtain the nuclear induction line shape. In particular, our MD results correctly indicate that gas phase spectra exhibit narrower lines at higher temperatures. (This is in contrast to conventional formalism, <sup>12–14</sup> which incorrectly predicts the opposite trend.) This work opens the door for the prediction of lineshapes in more complex geometries and boundary conditions. Our work differs from previous studies of diffusion<sup>49</sup> in that memory effects can be explicitly modeled using our method. Future directions may include explicit modeling of boundaries and gas types using appropriate memory kernels and, ultimately, solving the inverse problem of computing molecular and pore parameters from experimentally measured nuclear induction decays.

#### **ACKNOWLEDGMENTS**

This work used computational and storage services associated with the Hoffman2 Shared Cluster provided by the UCLA Institute for Digital Research and Education's Research Technology Group. L.-S.B. acknowledges funding from NSF Award No. CHE-2002313.

#### **AUTHOR DECLARATIONS**

#### **Conflict of Interest**

The authors have no conflicts to disclose.

## **Author Contributions**

Mohamad Niknam: Conceptualization (equal); Formal analysis (equal); Investigation (equal); Validation (equal); Writing - original draft (equal). Louis-S. Bouchard: Conceptualization (equal); Formal analysis (equal); Funding acquisition (equal); Project administration (equal); Supervision (equal); Writing - review & editing (equal).

## **DATA AVAILABILITY**

The data that support the findings of this study are available from the corresponding author upon reasonable request. LAMMPS code for conducting MD simulations, a sample of data

files, and a Python code for analyzing the results can be accessed at https://doi.org/10.5061/dryad.0p2ngf26k.

#### **REFERENCES**

- <sup>1</sup>E. Hahn, "Spin echoes," Phys. Rev. **80**, 580-594 (1950).
- <sup>2</sup>P. Mansfield, "Multi-planar image formation using NMR spin echoes," J. Phys. C: Solid State Phys. 10, L55 (1977).
- <sup>3</sup>P. C. Lauterbur, "Image formation by induced local interactions: Examples employing nuclear magnetic resonance," Nature 242, 190–191 (1973).
- <sup>4</sup>D. A. Yablonskiy, A. L. Sukstanskii, and J. D. Quirk, "Diffusion lung imaging with hyperpolarized gas MRI," NMR Biomed. 30, e3448 (2017).
- <sup>5</sup>A. A. Lysova and I. V. Koptyug, "Magnetic resonance imaging methods for in situ studies in heterogeneous catalysis," Chem. Soc. Rev. 39, 4585-4601 (2010).
- <sup>6</sup>L. F. Gladden, "Applications of in situ magnetic resonance techniques in chemical reaction engineering," Top. Catal. 8, 87-95 (1999).
- <sup>7</sup>N. Jarenwattananon et al., "Thermal maps of gases in heterogeneous reactions," Nature 502, 537-540 (2013).
- <sup>8</sup>D. van Dusschoten, C. T. Moonen, P. A. De Jager, and H. Van As, "Unraveling  $diffusion\ constants\ in\ biological\ tissue\ by\ combining\ Carr-Purcell-Meiboom-Gill$ imaging and pulsed field gradient NMR," Magn. Reson. Med. 36, 907-913 (1996).
- <sup>9</sup>E. C. Qin et al., "Combining MR elastography and diffusion tensor imaging for the assessment of anisotropic mechanical properties: A phantom study," J. Magn. Reson. Imaging 37, 217–226 (2013).
- <sup>10</sup>N. Jarenwattananon and L.-S. Bouchard, "Motional averaging of nuclear resonance in a field gradient," Phys. Rev. Lett. 114, 197601 (2015).
- <sup>11</sup>N. Jarenwattananon and L.-S. Bouchard, "Breakdown of Carr-Purcell Meiboom-Gill spin echoes in inhomogeneous fields," J. Chem. Phys. 149, 084304 (2018).
- <sup>12</sup>B. Herzog and E. L. Hahn, "Transient nuclear induction and double nuclear resonance in solids," Phys. Rev. 103, 148-166 (1956).
- <sup>13</sup>D. Pfitsch, A. McDowell, and M. S. Conradi, "What are the conditions for exponential time-cubed echo decays?," J. Magn. Reson. 139, 364-370 (1999).
- <sup>14</sup>C. Slichter, Principles of Magnetic Resonance (Springer, 1990).
- <sup>15</sup>T. Li and M. Raizen, "Brownian motion at short time scales," Ann. Phys. 525, 281-295 (2013).
- $^{16}\mathrm{V}.$  M. Starov and V. G. Zhdanov, "Effective viscosity and permeability of porous media," Colloids Surf., A 192, 363-375 (2001).
- <sup>17</sup>W.-P. Breugem, "The effective viscosity of a channel-type porous medium," Phys. Fluids 19, 103104 (2007).
- <sup>18</sup>V. Y. Rudyak and A. Belkin, "Molecular dynamics simulation of fluid viscosity in nanochannels," Nanosyst.: Phys., Chem., Math. 9, 349-355 (2018).
- <sup>19</sup>F. Rizk, S. Gelin, A.-L. Biance, and L. Joly, "Microscopic origins of the viscosity of a Lennard-Jones liquid," Phys. Rev. Lett. 129, 074503 (2022).
- <sup>20</sup>H. Carr and E. Purcell, "Effects of diffusion on free precession in nuclear magnetic resonance experiments," Phys. Rev. 94, 630-638 (1954).
- <sup>21</sup>H. Torrey, "Bloch equations with diffusion terms," Phys. Rev. 104, 563-565
- <sup>22</sup>P. Callaghan, Principles of Nuclear Magnetic Resonance Microscopy (Oxford,
- <sup>23</sup>E. Stejskal and J. E. Tanner, "Spin diffusion measurements: Spin echoes in the presence of a time-dependent field gradient," J. Chem. Phys. 42, 288-292 (1965).
- <sup>24</sup>P. Callaghan, Translational Dynamics and Magnetic Resonance (Oxford, 2011).
- <sup>25</sup>S. Meiboom and D. Gill, "Modified spin-echo method for measuring nuclear relaxation times," Rev. Sci. Instrum. 29, 688-691 (1958).
- <sup>26</sup>N. Jarenwattananon and L.-S. Bouchard, "Jarenwattananon and Bouchard reply," Phys. Rev. Lett. 117, 249702 (2016).
- <sup>27</sup>R. Zwanzig, Nonequilibrium Statistical Mechanics (Oxford University Press,
- <sup>28</sup>T. G. Mason, "Estimating the viscoelastic moduli of complex fluids using the
- generalized Stokes-Einstein equation," Rheol. Acta **39**, 371–378 (2000).

  <sup>29</sup>B. Haines and A. Mazzucato, "A proof of Einstein's effective viscosity for a dilute suspension of spheres," SIAM J. Math. Anal. 44, 2120-2145 (2012).

San Diego, 2002), Chap. 4, pp. 63-107.

- <sup>30</sup>M. Duerinckx and A. Gloria, "On Einstein's effective viscosity formula," arXiv:2008.03837 (2020).
- <sup>31</sup> A. Breki and M. Nosonovsky, "Einstein's viscosity equation for nanolubricated friction," Langmuir 34, 12968–12973 (2018).
- <sup>32</sup>R. Zwanzig and M. Bixon, "Hydrodynamic theory of the velocity correlation function," Phys. Rev. A 2, 2005 (1970).
- <sup>33</sup>T. G. Mason and D. A. Weitz, "Optical measurements of frequency-dependent linear viscoelastic moduli of complex fluids," Phys. Rev. Lett. **74**, 1250 (1995).
- <sup>34</sup> A. Córdoba, T. Indei, and J. D. Schieber, "Elimination of inertia from a generalized Langevin equation: Applications to microbead rheology modeling and data analysis," J. Rheol. **56**, 185–212 (2012).
- 35 S. Brush, "Theories of liquid viscosity," Chem. Rev. 62, 513 (1962).
- <sup>36</sup>R. Acosta *et al.*, "Diffusion in binary gas mixtures studied by NMR of hyperpolarized gases and molecular dynamics simulations," Phys. Chem. Chem. Phys. **8**, 4182–4188 (2006).
- <sup>37</sup>I.-C. Yeh and G. Hummer, "System-size dependence of diffusion coefficients and viscosities from molecular dynamics simulations with periodic boundary conditions," J. Phys. Chem. B 108, 15873–15879 (2004).
- <sup>38</sup> E. D. Hazelbaker *et al.*, "Combined application of high-field diffusion NMR and molecular dynamics simulations to study dynamics in a mixture of carbon dioxide and an imidazolium-based ionic liquid," J. Phys. Chem. B **116**, 9141–9151 (2012).
  <sup>39</sup> D. Frenkel and B. Smit, "Molecular dynamics simulations," in *Understanding Molecular Simulation*, 2nd ed., edited by D. Frenkel and B. Smit (Academic Press,

- <sup>40</sup>D. C. Rapaport, *The Art of Molecular Dynamics Simulation*, 2nd ed. (Cambridge University Press, 2004).
- <sup>41</sup> A. P. Thompson *et al.*, "LAMMPS: A flexible simulation tool for particle-based materials modeling at the atomic, meso, and continuum scales," Comput. Phys. Commun. **271**, 108171 (2022).
- <sup>42</sup>D. McQuarrie, *Statistical Mechanics* (Harper and Row, New York, 1975).
- <sup>43</sup>B. D. Todd and P. J. Daivis, Nonequilibrium Molecular Dynamics: Theory, Algorithms and Applications (Cambridge University Press, 2017).
- <sup>44</sup>H. J. Hanley, R. D. McCarty, and W. M. Haynes, "The viscosity and thermal conductivity coefficients for dense gaseous and liquid argon, krypton, xenon, nitrogen, and oxygen," J. Phys. Chem. Ref. Data 3, 979–1017 (1974).
- <sup>45</sup>S. Grisnik, "Measurement of xenon viscosity as a function of low temperature and pressure," in 34th AIAA/ASME/SAE/ASEE Joint Propulsion Conference and Exhibit (American Institute of Aeronautics and Astronautics, 1998), p. 3498.
- <sup>46</sup>R. Rowley and M. Painter, "Diffusion and viscosity equations of state for a Lennard-Jones fluid obtained from molecular dynamics simulations," Int. J. Thermophys. **18**, 1109–1121 (1997).
- <sup>47</sup>W. Haynes, D. Lide, and T. Bruno, CRC Handbook of Chemistry and Physics (CRC Press, 2016).
- <sup>48</sup> R. D. Mountain, "Molecular dynamics calculation of the viscosity of xenon gas," Int. J. Thermophys. 28, 259–267 (2007).
- <sup>49</sup>D. Grebenkov, "Paradigm shift in diffusion-mediated surface phenomena," Phys. Rev. Lett. 125, 078102 (2020).